Article

A 5000-Year Sedimentary Record of East Asian Winter Monsoon from the Northern Muddy Area of the East China Sea

Yanping Chen [1], Yan Li [2], Wenzhe Lyu [3], Dong Xu [4], Xibin Han [4], Tengfei Fu [3] and Liang Yi [5,*]

[1] Key Laboratory of Engineering Oceanography, Second Institute of Oceanography, Ministry of Natural Resources, Hangzhou 310012, China; chenai0812@163.com

[2] School of Ocean Sciences, China University of Geosciences, Beijing 100083, China; geo-liyan@foxmail.com

[3] Key Laboratory of Marine Sedimentology and Environmental Geology, First Institute of Oceanography, Ministry of Natural Resources, Qingdao 266062, China; lvwenzhe1992@gmail.com (W.L.); futengfei@fio.org.cn (T.F.)

[4] Key Laboratory of Submarine Geosciences, Second Institute of Oceanography, Ministry of Natural Resources, Hangzhou 310012, China; xudongsio@126.com (D.X.); hanxibin@sio.org.cn (X.H.)

[5] State Key Laboratory of Marine Geology, Tongji University, Shanghai 200092, China

* Correspondence: yiliang@tongji.edu.cn

check for updates

Abstract: The variability of the winter monsoon is one of the key components of the Asian monsoon, significantly influencing paleoenvironmental evolution in East Asia. However, whether the winter or the summer monsoon is the dominated factor controlling sedimentary dynamics of the muddy areas of the continental shelves of the East China Sea is debated, due to lack of consistency between various winter monsoon proxies in previous studies. In this work, the sediments of the upper part of core ECS-DZ1 with several marine surface samples were studied in terms of sediment grain size and radiocarbon dating, and changes in sedimentary dynamics of the northern muddy area of the ECS over the past 5000 years were documented. The main findings are as follows: (1) regional sedimentary dynamics were low and did not significantly change since the middle Holocene; (2) coarse particles are the dominated component in the sediments; (3) a proxy can be derived to indicate changes in winter monsoon. Based on this reconstructed winter monsoon record, we found that this record was generally negatively correlated to the stalagmite-based summer monsoon variability over the past 3500 years, but positively correlated before that. Moreover, this record can be well correlated to changes in the Kuroshio Current and the Bond ice-rafting debris events in the North Atlantic on millennial timescales, inferring large-scale and common atmospheric dynamics across the Asian continent over the past 5000 years. Therefore, we concluded that the winter monsoon is the predominant factor controlling sedimentary dynamics in the northern part of the ECS and proposed that the contribution of coarse particles may be one of potential indices to identify the role of the winter and the summer monsoons in sedimentary evolution.

Keywords: East China Sea; middle to late Holocene; sediment grain size; East Asian winter monsoon; sedimentary dynamics

1. Introduction

The East China Sea (ECS) is located between the Asian continent to the west and the Pacific Ocean to the east, with an area of 770,000 km^2 (Figure 1). The ECS is influenced by the monsoonal system and the Kuroshio Current (KC) and the Zhe-Min coastal currents, and the ECS basin has been infilling by terrigenous materials carried by the Changjiang (Yangtze), Huanghe, and other regional rivers

(Figure 1). During summers, sediment flux from rivers into the sea is high, whereas the coastal currents are weak [1,2], and during winters, sediments from the Changjiang estuary and the Zhe-Min coastal areas are transported seaward by strong winds and waves [3,4].
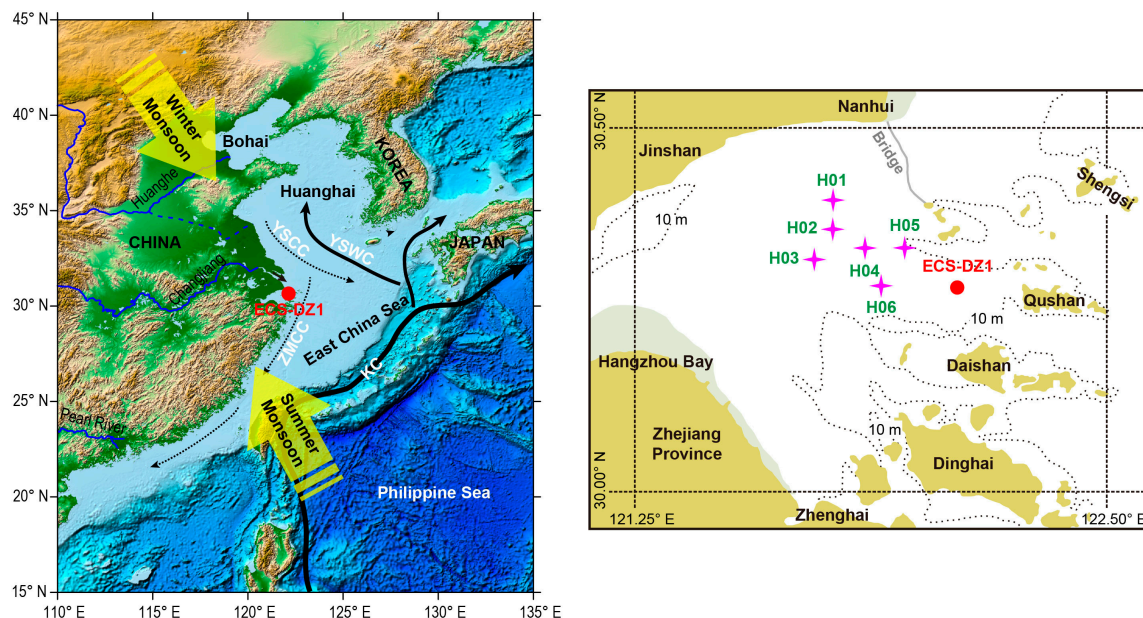

Figure 1. Location of core ECS-DZ1 with 6 sites of surface samples (H1-H6) and regional climatic and oceanographic systems. The solid arrows denote warm currents (YSWC, Yellow Sea warm current; KC, Kuroshio current), and the dashed arrows indicate coastal cold waters (YSCC, Yellow Sea coast cold water). The base map data was generated using the open and free software DIVA-GIS 7.5 (http://www.diva-gis.org/).

Within the continental shelves and along the coastal zones of the ECS, several mud areas developed during the Holocene [5], with high sediment fluxes and high depositional rates (Figure 1). These sediments are potentially valuable for understanding the role of continental shelves in transporting detrital materials from land to deep ocean [6,7]. Over the past decades, many researchers attempted to link sedimentary processes there to the past changes in sea level, Asian monsoon, deltaic developments and ocean currents [8–10]. For instance, Zhang, et al. [11] combined sedimentary dynamics and geochemical properties of the north inner continental shelf of the ECS and quantitatively reconstructed the East Asian winter monsoon (EAWM) in the last century. Lyu, et al. [12] claimed a mechanism that how Arctic winter climates modulated the relationship between the East Asian summer monsoon (EASM) and the Yellow Sea Warm Current (YSWC) over the past 1500 years, by an integration of sedimentary dynamics and mineralogical properties of the central Bohai Sea. These two new records are somehow conflicted—whether the EAWM or the EASM dominates the sedimentary processes of muddy areas on the continental shelves—and the potential mechanism has been hotly debated in the past decade, because of the large difference between published monsoonal proxies [1,4,13]. The mechanism may be locality-specific [14,15]; however, the criterion for assessing the locality is absent, since modern observations highlight the seasonality of different sedimentary factors [16,17]. Therefore, documenting monsoonal variabilities from sedimentary sequences of various localities and timescales is important to clarify the dominant dynamics in sedimentation on the continental shelves and thus contribute to understand the teleconnection between different climatic systems.

In this study, the upper part of core ECS-DZ1 (Figure 1) was studied by changes in sediment grain size and radiocarbon dating. An EAWM proxy was derived to analyze climatic influences on sedimentary processes in the northern muddy area of the ECS over the past 5000 years. Based on

these results and comparisons with previously published results in the muddy areas of the ECS, the dominated factors in sedimentary dynamics in the study area were discussed.

2. Core ECS-DZ1 and Experiments

The study area locates at the Zhoushan Islands, northwest of the ECS (Figure 1), with an annual temperature of 15.8–16.7 °C, an annual rainfall of 920–1320 mm, and an annual evaporation of 1200–1400 mm. Core ECS-DZ1 (30°29′ N, 112°03′ E, water depth 12 m) was drilled in the summer of 2012, with a length of 153.6 m and a recovery rate of ~90%. The core contained fluvial and marine sediments and was study in terms of magnetostratigraphy and luminescence dating to reconstruct tectonic activities of the Zhe-Min Uplift in the Quaternary [18] and to recover regional sea level changes in the last deglaciation [19].

The upper 55 m is composed of alternations between thick grey silt layer (3–8 cm) and thin coarser layer (0.5–1.0 cm), inferring a marine environment of subtidal or shallow sea [18]. These deposits were dated to the last deglaciation and the Holocene by luminescence methods [19]. Accordingly, the upper 2.8 m mainly contains fluid mud with a high-water content, and 11.8 m in depth is a sedimentary boundary with ~4 kyr hiatus [19]. Thus, we sampled the sediments in 2.8–11.8 m depth with 0.1-m interval to study sedimentary dynamics over the past 5000 years. Moreover, to clarify the significance of sediment grain-size variability of core ECS-DZ1, marine surface sediments from six sites were collected for references (Figure 1).

Four samples were collected for radiocarbon dating. Organic carbon from organic matters in the sediments was extracted and measured at Beta Analytic Inc. USA using the Accelerator Mass Spectrometry method (AMS). To identify reservoir effects of dating organic carbons in the sediments, a comparison was conducted with a luminescence age [19], and all radiocarbon dates were calibrated using the age difference between these two methods.

Ninety-one borehole samples and six surface sediments were pretreated with 10–20 mL of 30% H_2O_2 to remove organic matter, washed with 10% HCl to remove carbonates and mollusk fragments, rinsed with deionized water, and then placed in an ultrasonic vibrator for several minutes to facilitate dispersion. Grain-size spectra with one hundred grain-size classes between 0.3 and 700 µm were measured using a Malvern Mastersizer 2000 grain size analyzer installed at the Second Institute of Oceanography.

Grain-size analysis of the sediments is a useful and effective tool for various sedimentary and paleoenvironmental inferences, e.g., [20–23]. To identify the processes controlling sediment grain size changes and to extract potential paleoenvironmental signals, we analyzed sediment grain-size spectra through varimax-rotated, principal component analysis (VPCA), which can partition various sediment inputs or dynamics components [24,25]. This method assumes that each sedimentary process is related with a specific grain-size spectral shape. Similarly, polymodal grain-size spectra can be mathematically partitioned [26], following a particular theoretical distribution [27–29]. These two methods allow us to separate out orthogonal modes (independent grain-size spectral components/factors) and thus to identify potential changes of input functions [24,25,30]. The exported one hundred grain-size classes between 0.3 and 700 µm were used for the two analyses.

3. Results

3.1. Age-Depth Model

In general, four radiocarbon dates are stratigraphically consistent (Table 1), and the correlation coefficient between ages and depths is r = 0.99 (n = 4, p < 0.01); this indicates that the sediment accumulation rate was relatively constant. To identify reservoir effects in dating organic carbons, we used this linear regression to extrapolate an age for 5.8 m depth, that is ~3800 yr BP. This extrapolating age is 2500 years older than the luminescence age (1300 yr BP) [19]. Unlike radiocarbon dating on foraminifera, dating organic carbons in the sediments is usually influenced by the input of old organic

carbon by rivers and currents, e.g., [31–33]. To remove this old-carbon influence in previous studies, the age difference between two dating methods on the same sample should be determined; and in this study, the value is ~2500 year. Thus, subtracting the reservoir effect of organic carbons (~2500 years) from the original radiocarbon dates, an age-depth model was established using a regression model by fitting the all five ages (Figure 2), yielding an age of 4819 ± 307 yr BP for 11.8 m in depth.

Table 1. Radiocarbon dating on the organic materials from core ECS-DZ1.

Lab No.	Depth (m)	Conventional Age ± Error (y BP)	Reservoir Effect (Years)	Calibrated Age (cal y BP)
375,194	7.1	4760 ± 30	2021 ± 95	1841–2246
375,193	7.4	4850 ± 30	4477 ± 106	4244–4713
375,195	8.6	5880 ± 30	5106 ± 116	4879–5290
375,196	10.5	6940 ± 40	6448 ± 90	6289–6621
[1] NL-291	5.8	1300 ± 200	-	-

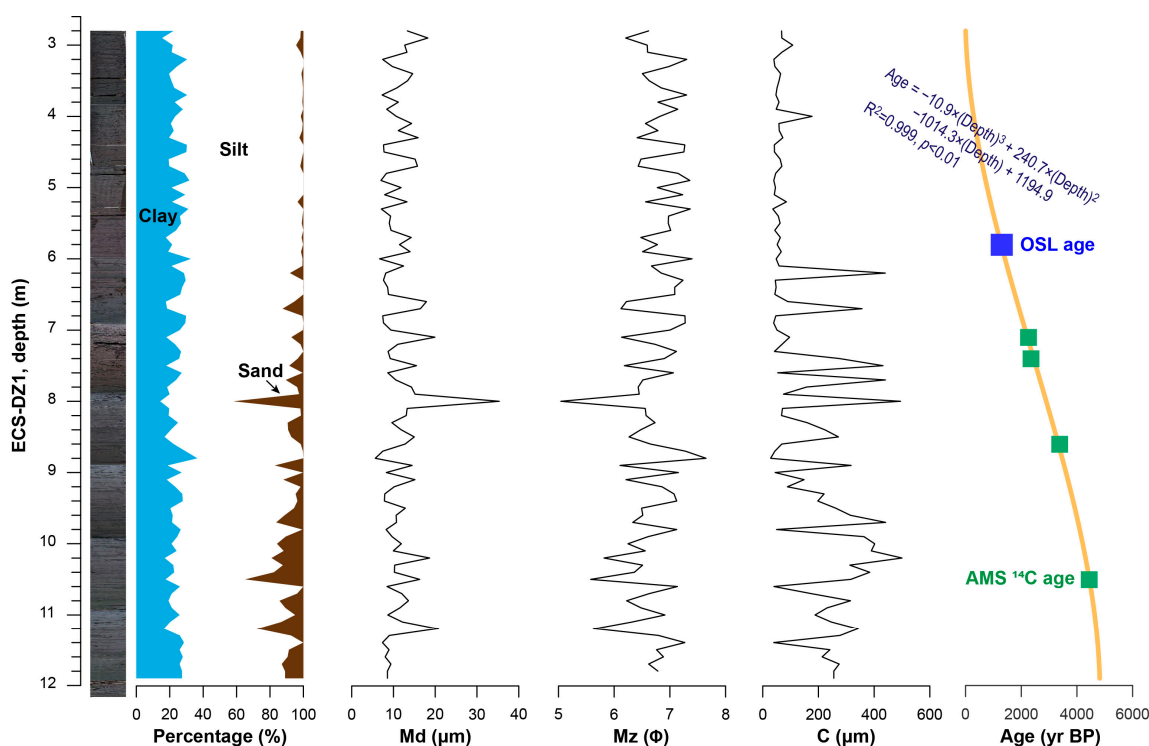[1] A luminescence age from Wang et al. [19].

Figure 2. Core photos and profile of core ECS-DZ1 about component percentages of clay (<4 μm), silt (4–63 μm), and sand (>63 μm), median size (Md), mean size (Mz), C value (the one percentile of grain size distribution), and AMS 14C dating results with an age-depth model.

3.2. Sediment Grain-Size

Throughout the studied interval of core ECS-DZ1 (2.8–11.8 m), the mean value of sediment grain size (Mz) is 6.7 ± 0.5 Φ, which indicates a low-dynamic sedimentary process that did not significantly change during the past ~5000 years (Figure 2). We observed that clay (<4 μm) and silt (4~63 μm) particles changed little with average values of 23.6 ± 4.5%, and 71.1 ± 6.8%, respectively, while the variance of sand (>63 μm) particles is relatively large with an average value of 5.4 ± 7.6%. This can be similarly observed in C values, which represents the one percentile of grain size distribution.

To identify the characterized dynamic components, two parameters were selected: C value, representing the most hydrodynamic sedimentary component, and Md, the median diameter,

indicating the mean hydrodynamic energy. The C-M diagram can provide valuable insights into sediment transport and hydrodynamic intensity [34,35]. As shown, prior to 2000 y BP, the most dynamic sedimentary process recorded in core ECS-DZ1 did not follow changes in the dominant sedimentary components or dynamics, while after 2000 yr BP, these two parameters were coupled (Figure 3b). For suspended and sea-surface sediments around the Huanghe River mouth [36] and the mud area of the Bohai Sea [12], a good positive correlation between C and Md values was observed, similarly with ones of core Lz908 [37], and ones in the abandoned Huanghe River mouth in the west of the South Yellow Sea [38]. This relationship was consistent in the one of six surface sediments (Figure 3). It is subsequently inferred that the most dynamic component in core ECS-DZ1 since 2000 y BP was integrated into continental shelf deposition with the mean state of various sedimentary processes, similarly in the first proposed C-M diagram in studying the sediments of various sedimentary facies and depositional periods [34,35]. However, prior to 2000 y BP, C and Md values varied somehow independently, inferring that the most dynamic component-coarse particles-significantly strengthened.
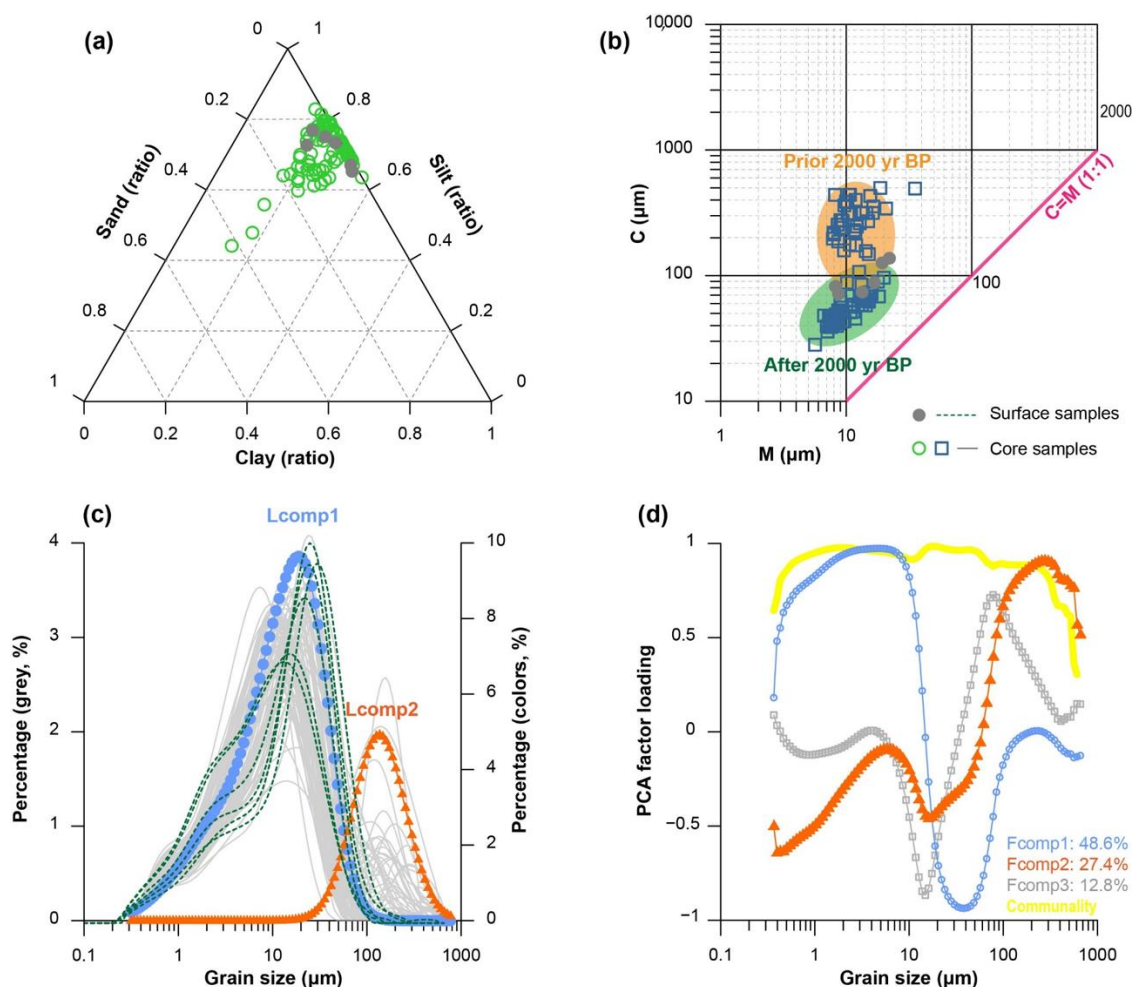

Figure 3. Characteristics of sediment grain size of core ECS-DZ1 and six surface samples. (**a**) Ternary diagrams; (**b**) C-M diagrams; (**c**) grain size distribution; (**d**) principal component analysis. Lcomp1 and Lcomp2 are the two characterized grain-size components through mathematical partitioning of sediment grain-size spectrum; and Fcomp1, Fcomp2, and Fcomp3 are the three components by VPCA.

For grain-size distribution, a multi-mode pattern was observed, which agrees well with modern samples and did not change significantly during the past 5000 years (Figure 3c). VPCA results identify three characteristic components, which accounts for 88.9% of the total variance (Table 2). According to

their eigenvalues (Figure 3d), the first two leading components (Fcomp1 and Fcomp2) likely integrate variations of low- and high-dynamic sedimentary processes, respectively; and for the third component (Fcomp3), it seems that this is complementary to the first two leading components. Furthermore, employing a three-component lognormal function, all the measured grain-size data in one hundred grain-size classes can be unmixed [23]. As a result, all data of sediment grain-size spectrum can be fitted by three components. Because the modes of the two finer components are overlapped, we combine them together and obtain two characterized records, i.e., Lcomp1 and Lcomp2, representing low- and high-dynamic sedimentary processes, respectively (Figure 3c). The integration of all these lines of evidence highlights the contribution of high-dynamic processes in the sediments and the dominance of sandy particles with a greater variance in core ECS-DZ1.

Table 2. Results of principal component analysis of sediment grain-size of core ECS-DZ1.

Component	Initial Eigenvalues/Extraction Sums of Squared Loadings		
	Total	% of Variance	Cumulative %
Fcomp1	46.71	48.65	48.65
Fcomp2	26.30	27.40	76.05
Fcomp3	12.30	12.81	88.86
. . . .	. . . .	. . . .	. . . .

4. Discussion

By analyzing sedimentary dynamics of the study area, the monsoonal influence can be recovered, thus reconstructing the monsoonal history over the past 5000 years. As shown, except for Fcomp1, changes in most of grain-size parameters are similar (Figure 4), which may indicate that the fine-grained particles in core ECS-DZ1 did not significantly change and the coarse-grained particles were the dominated component. The consistency between various grain-size parameters is similar and can be improved after a moving average calculation (Figure 5a).

According to this consistency, the Fcomp2 record was employed to represent changes in sedimentary dynamics and compared with various paleoenvironmental proxies of climatic changes in East Asia. As a result (Figure 4), the Fcomp2 varies considerably, and its variation can be generally divided into two subgroups, namely a greater variance prior to ~2000 y BP and a significant decrease since then. In addition, a persistent decrease of sedimentary dynamics over the past ~5000 year was observed, which agrees well with the long-term trend of the EAWM identified in a transient simulation [39]. The Fcomp2 is also consistent with a recently published record of the EAWM in Central Asia [40]. All these evidences infer the possibility of the Fcomp2 as a proxy of the EAWM and highlight orbital forcing in regional climatic changes on millennial timescales.
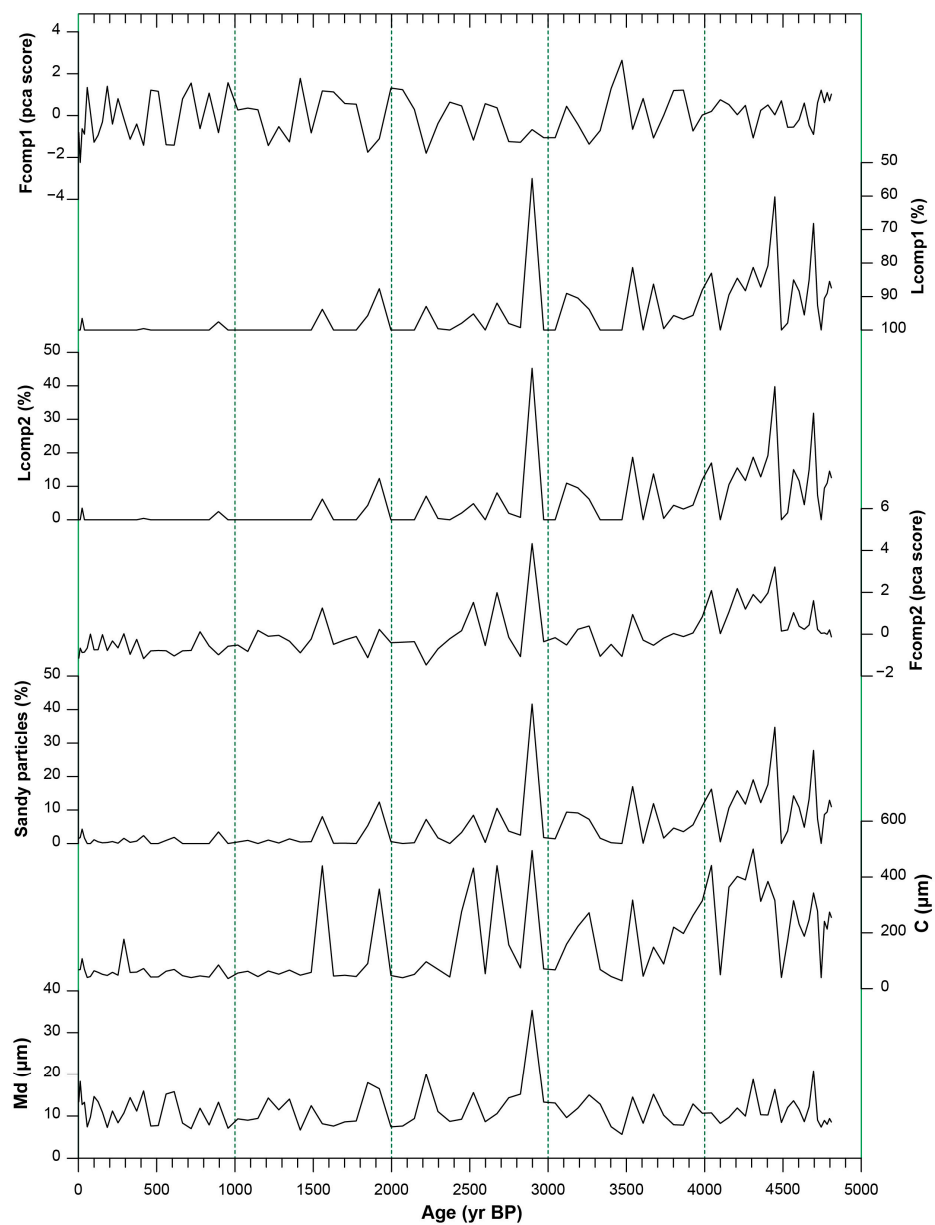
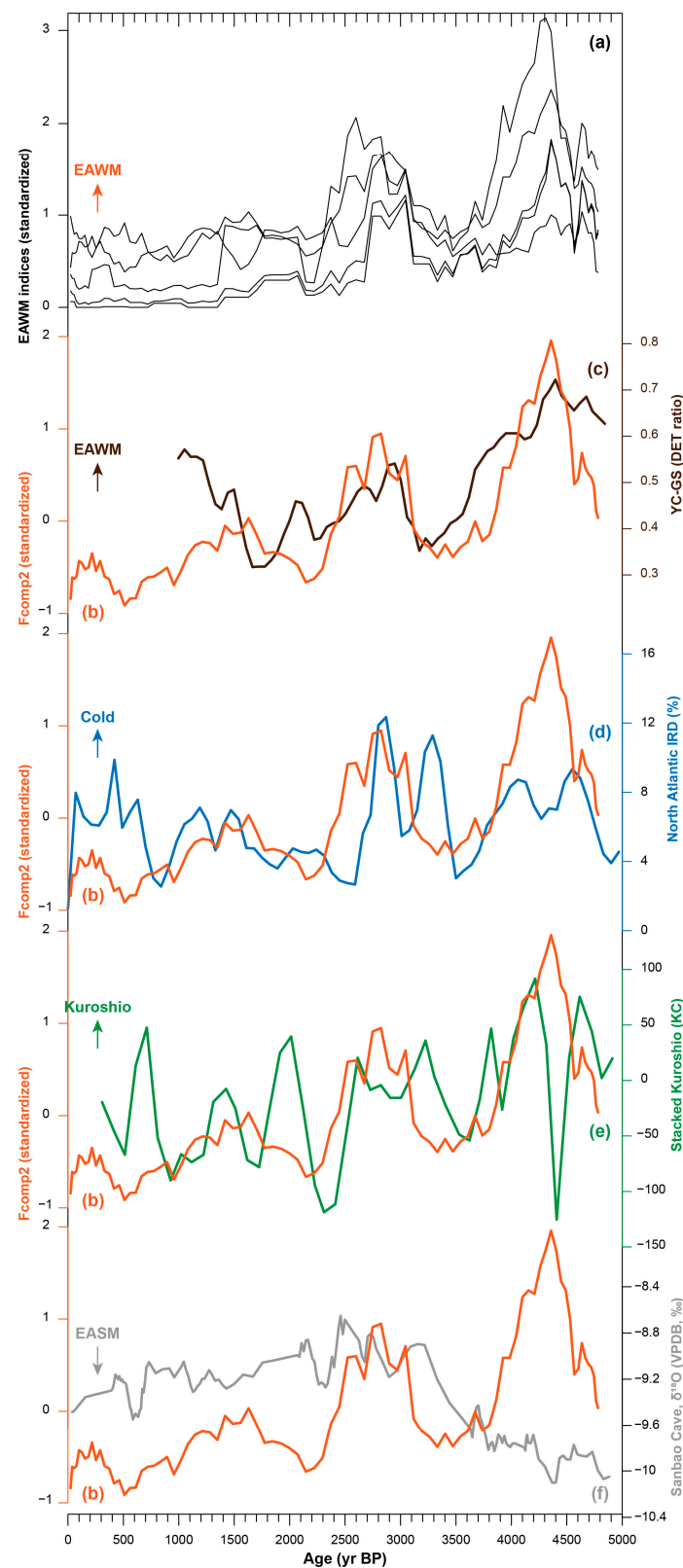**Figure 4.** Changes in sediment grain-size parameters of core ECS-DZ1.

Figure 5. Comparison between various paleoenvironmental proxies over the past 5000 years. (**a**) 5-point moving average of five grain-size parameters of core ECS-DZ1; (**b**) Fcom2 record of core ECS-DZ1 indicating changes in the winter monsoon; (**c**) DET YS-GS index, indicating winter dust storms in Central Asia [40]; (**d**) ice-rafting debris (IRD), stack ice-rafting debris data from Bond, et al. [41]; (**e**) Stack KC, integrated indicator from four time series [42]; (**f**) Stalagmite δ18O series of Sanbao Cave [43], indicating East Asian summer monsoon (EASM) intensity.

Moreover, changes in regional sedimentary dynamics in the study area (Fcomp2) are well correlated to the Bond ice-rafting debris (IRD) events (Figure 5b), which were expressed in the North Atlantic when large numbers of icebergs discharging from the Labrador Sea and Baffin Bay. The Bond IRD events represent a major climate state of high-latitude areas of the Northern Hemisphere on millennial timescales [41,44], and play a critical role in winter climates across the East Asia, e.g., [12,40,45], thus inferring a tightened and rapid atmospheric teleconnection between the North Atlantic and the Asian monsoon [43,46,47]. Similarly, the Fcomp2 can be also linked to the Kuroshio Current (Figure 5c), which is the most important component of the subtropical North Pacific gyre in winters influencing climate changes in the western Pacific [48]. These two factors are critical to winter conditions of eastern China [49,50], and the agreement between these three proxies demonstrates a large-scale and common atmospheric pattern across the Asian continent over the past 5000 years.

The EAWM variability is one of the key components of Asian monsoon, and based on the pedogenesis of Chinese loess-paleosol sequences [51–53], a large number of EAWM records in terms of Holocene and Pleistocene dynamics have been recovered from deposits of lakes and continental shelves [4,13,51–55]. For the sediments on the continental shelves of the ECS, the basic hypothesis is that offshore currents triggered by the EAWM is the predominant dynamics for these deposits [1,4,13]. However, there is no much consistency in the Holocene between the proposed EAWM records in the continental shelves, likely due to the influence of the greater flux by rivers to the continental shelves in summers, which is another key factor influencing sedimentary dynamics in these muddy areas. Hence, some researchers claimed that the EASM could be a unignored factor dominating sedimentary dynamics in the muddy areas of the Bohai Sea and the South Yellow Sea [12,15].

To assure the difference of various monsoonal records, we reviewed these published cores and found that the sediments dominated by the EASM are relatively finer. In specific, for EASM records, the Md values of core M38002 from the South Yellow Sea range 8–14 μm [15], and the ones of core B60 from the Bohai Sea are 10–40 μm [12]; For EAWM records, a sandy component (>100 μm) significantly contributes in sediment grain-size changes ([11,13]; and this study). Although it needs more evidence to verify its reliability in future, this observation agrees well with modern sedimentary dynamics in the continental shelves of the ECS [16,17], namely strong northerly winds and storm surges in winters and higher sediment fluxes in summers. Thus, we claim that the EAWM is the predominant factor controlling sedimentary dynamics in the northern part of the ECS, and propose that coarse particles in sediment grain-size distributions may be one of the potential indices to identify the role of the EAWM and the EASM in sedimentary dynamics on the continental shelves of the ECS.

Furthermore, the EAWM proxy derived from coarse particles of core ECS-DZ1 provide an opportunity to test the relationship between winter and summer monsoons. An anti-phase relation between the EAWM and the EASM on orbital timescales has been identified by various types of monsoonal records [53], while in the Holocene, their relationship is debated [54,56–58], likely due to pedogenic disturbances, diagenetic modifications and/or dating issues [51]. In this study, our EAWM record was generally negatively correlated to the stalagmite-based EASM variability over the past 3500 years, and positively correlated between 5000 y BP and 3500 y BP (Figure 5). This obversion is consistent with that the synchronization between the EAWM and the EASM before the middle Holocene and the reversed relationship since the middle Holocene [53]. The changing relationship between the EASM and the EAWM demonstrates the complexity within the monsoon system, which was likely resulted from the role of summer insolation during different intervals [53,56]. Therefore, we concluded that our study highlights the potential of recovering the monsoonal variability from the muddy areas on the continental shelves of the ECS and of testing the relationships of winter and summer monsoons in different intervals.

5. Conclusions

By studying the upper part (2.8–11.8 m) of core ECS-DZ1 in terms of sediment grain size and radiocarbon dating, together with modern surface samples, changes in sedimentary dynamics of the

northern muddy area of the ECS over the past 5000 years were documented. We found that the mean value of sediment grain size (Mz) is $6.7 \pm 0.5 \, \Phi$, and clay and silt particles changed little with average values of $23.6 \pm 4.5\%$ and $71.1 \pm 6.8\%$, respectively, while the variance of sand particles is relatively large with an average value of $5.4 \pm 7.6\%$. The variability of these sediment grain-size parameters infers a low-dynamic sedimentary process that did not significantly change over the past ~5000 years, and that the sandy particles was the dominated component in the sediments. According to these observations, a coarse-grain based proxy was derived to indicate changes in the EAWM. This EAWM record agrees well with the one of Central Asia, and can be well correlated to changes in the Kuroshio Current and the Bond IRD events in the North Atlantic on millennial timescales. Moreover, our EAWM record was generally negatively correlated to the stalagmite-based EASM variability over the past 3500 years, but positively correlated before that. Therefore, we concluded that the EAWM is the predominant factor controlling sedimentary dynamics in the northern part of the ECS and proposed that the contribution of coarse particles in sediment grain-size distributions may be one of the potential indices to identify the role of the EAWM and the EASM in sedimentary evolution.

Conflicts of Interest: The authors declare no conflict of interest.

References

1. Hu, L.M.; Lin, T.; Shi, X.F.; Yang, Z.S.; Wang, H.J.; Zhang, G.; Guo, Z.G. The role of shelf mud depositional process and large river inputs on the fate of organochlorine pesticides in sediments of the Yellow and East China seas. *Geophys. Res. Lett.* **2011**, *38*. [CrossRef]
2. Wang, Y.; Cheng, H.; Edwards, R.L.; He, Y.; Kong, X.; An, Z.; Wu, J.; Kelly, M.J.; Dykoski, C.A.; Li, X. The Holocene Asian Monsoon: Links to Solar Changes and North Atlantic Climate. *Science* **2005**, *308*, 854–857. [CrossRef] [PubMed]
3. Liu, J.P.; Xu, K.H.; Li, A.C.; Milliman, J.D.; Velozzi, D.M.; Xiao, S.B.; Yang, Z.S. Flux and fate of Yangtze River sediment delivered to the East China Sea. *Geomorphology* **2007**, *85*, 208–224. [CrossRef]
4. Xiao, S.; Li, A.; Liu, J.P.; Chen, M.; Xie, Q.; Jiang, F.; Li, T.; Xiang, R.; Chen, Z. Coherence between solar activity and the East Asian winter monsoon variability in the past 8000 years from Yangtze River-derived mud in the East China Sea. *Palaeogeogr. Palaeoclimatol. Palaeoecol.* **2006**, *237*, 293–304. [CrossRef]
5. Bian, C.; Jiang, W.; Greatbatch, R.J. An exploratory model study of sediment transport sources and deposits in the Bohai Sea, Yellow Sea, and East China Sea. *J. Geophys. Res. Oceans* **2013**, *118*, 5908–5923. [CrossRef]
6. Gao, S.; Wang, D.; Yang, Y.; Zhou, L.; Zhao, Y.; Gao, W.; Han, Z.; Yu, Q.; Li, G. Holocene sedimentary systems on a broad continental shelf with abundant river input: Process–product relationships. *Geol. Soc. Lond. Spec. Publ.* **2016**, *429*, 223–259. [CrossRef]
7. Qiao, S.; Shi, X.; Wang, G.; Zhou, L.; Hu, B.; Hu, L.; Yang, G.; Liu, Y.; Yao, Z.; Liu, S. Sediment accumulation and budget in the Bohai Sea, Yellow Sea and East China Sea. *Mar. Geol.* **2017**, *390*, 270–281. [CrossRef]
8. Liu, J.P.; Milliman, J.D.; Gao, S.; Cheng, P. Holocene development of the Yellow River's subaqueous delta, North Yellow Sea. *Mar. Geol.* **2004**, *209*, 45–67. [CrossRef]
9. Peng, J.; Luo, X.; Liu, F.; Zhang, Z. Analysing the influences of ENSO and PDO on water discharge from the Yangtze River into the sea. *Hydrol. Process.* **2018**, *32*, 1090–1103. [CrossRef]
10. Yang, Z.S.; Liu, J.P. A unique Yellow River-derived distal subaqueous delta in the Yellow Sea. *Mar. Geol.* **2007**, *240*, 169–176. [CrossRef]

11. Zhang, X.; Fan, D.; Tian, Y.; Sun, Z.; Zhai, B.; Liu, M.; Chen, B.; Yang, Z. Quantitative reconstruction of the East Asian Winter Monsoon evolution over the past 100 years: Evidence from high-resolution sedimentary records of the inner continental shelf of the East China Sea. *Holocene* **2020**, *30*, 1053–1062. [CrossRef]

12. Lyu, W.; Yang, J.; Fu, T.; Chen, Y.; Hu, Z.; Tang, Y.Z.; Lan, J.; Chen, G.; Su, Q.; Xu, X.; et al. Asian monsoon and oceanic circulation paced sedimentary evolution over the past 1500 years in the central mud area of the Bohai Sea, China. *Geol. J.* **2020**, *55*, 5606–5618. [CrossRef]

13. Qiao, S.; Yang, Z.; Liu, J.; Sun, X.; Xiang, R.; Shi, X.; Fan, D.; Saito, Y. Records of late-Holocene East Asian winter monsoon in the East China Sea: Key grain-size component of quartz versus bulk sediments. *Quat. Int.* **2011**, *230*, 106–114. [CrossRef]

14. Zhou, X.; Sun, L.; Huang, W.; Liu, Y.; Jia, N.; Cheng, W. Relationship between magnetic susceptibility and grain size of sediments in the China Seas and its implications. *Cont. Shelf Res.* **2014**, *72*, 131–137. [CrossRef]

15. Zhou, X.; Sun, L.; Huang, W.; Cheng, W.; Jia, N. Precipitation in the Yellow River drainage basin and East Asian monsoon strength on a decadal time scale. *Quat. Res.* **2012**, *78*, 486–491. [CrossRef]

16. Liu, X.Q. *Marine Environmental Geology of China*; Ocean Press: Beijing, China, 2006.

17. Yuan, D.; Hsueh, Y. Dynamics of the cross-shelf circulation in the Yellow and East China Seas in winter. *Deep Sea Res. Part II Top. Stud. Oceanogr.* **2010**, *57*, 1745–1761. [CrossRef]

18. Yi, L.; Ye, X.; Chen, J.; Li, Y.; Long, H.; Wang, X.; Du, J.; Zhao, S.; Deng, C. Magnetostratigraphy and luminescence dating on a sedimentary sequence from northern East China Sea: Constraints on evolutionary history of eastern marginal seas of China since the Early Pleistocene. *Quat. Int.* **2014**, *349*, 316–326. [CrossRef]

19. Wang, Y.; Long, H.; Yi, L.; Yang, L.; Ye, X.; Shen, J. OSL chronology of a sedimentary sequence from the inner-shelf of the East China Sea and its implication on post-glacial deposition history. *Quat. Geochronol.* **2015**, *30*, 282–287. [CrossRef]

20. Yi, L.; Yu, H.J.; Ortiz, J.D.; Xu, X.Y.; Qiang, X.K.; Huang, H.J.; Shi, X.; Deng, C.L. A reconstruction of late Pleistocene relative sea level in the south Bohai Sea, China, based on sediment grain-size analysis. *Sediment. Geol.* **2012**, *281*, 88–100. [CrossRef]

21. Ma, L.; Abuduwaili, J.; Liu, W.; He, Z. Variations in Sediment Grain Size from a Lake in the Tianshan Mountain of Central Asia: Implications for Paleoprecipitation Reconstruction. *Appl. Sci.* **2020**, *10*, 6793. [CrossRef]

22. Wang, C.; Chen, M.; Qi, H.; Intasen, W.; Kanchanapant, A. Grain-Size Distribution of Surface Sediments in the Chanthaburi Coast, Thailand and Implications for the Sedimentary Dynamic Environment. *J. Mar. Sci. Eng.* **2020**, *8*, 242. [CrossRef]

23. Paterson, G.A.; Heslop, D. New methods for unmixing sediment grain size data. *Geochem. Geophys. Geosyst.* **2015**, *16*, 4494–4506. [CrossRef]

24. Yi, L.; Yu, H.-J.; Ortiz, J.D.; Xu, X.-Y.; Chen, S.-L.; Ge, J.-Y.; Hao, Q.-Z.; Yao, J.; Shi, X.-F.; Peng, S.-Z. Late Quaternary linkage of sedimentary records to three astronomical rhythms and the Asian monsoon, inferred from a coastal borehole in the south Bohai Sea, China. *Palaeogeogr. Palaeoclimatol. Palaeoecol.* **2012**, *329–330*, 101–117. [CrossRef]

25. Darby, D.A.; Ortiz, J.; Polyak, L.; Lund, S.; Jakobsson, M.; Woodgate, R.A. The role of currents and sea ice in both slowly deposited central Arctic and rapidly deposited Chukchi–Alaskan margin sediments. *Glob. Planet. Chang.* **2009**, *68*, 58–72. [CrossRef]

26. Ashley, G.M. Interpretation of polymodal sediments. *J. Geol.* **1978**, *86*, 411–421. [CrossRef]

27. Kranck, K.; Smith, P.C.; Milligan, T.G. Grain-size characteristics of fine-grained unflocculated sediments I: 'one-round' distributions. *Sedimentology* **1996**, *43*, 589–596. [CrossRef]

28. Kranck, K.; Smith, P.C.; Milligan, T.G. Grain-size characteristics of fine-grained unflocculated sediments II:'milti-round' distributions. *Sedimentology* **1996**, *43*, 597–606. [CrossRef]

29. Påsse, T. Grain size distribution expressed as tanh-functions. *Sedimentology* **1997**, *44*, 1011–1014. [CrossRef]

30. Weltje, G.J. End-member modeling of compositional data: Numerical-statistical algorithms for solving the explicit mixing problem. *Math. Geol.* **1997**, *29*, 503–549. [CrossRef]

31. Chen, H.; Zhu, L.; Ju, J.; Wang, J.; Ma, Q. Temporal variability of 14C reservoir effects and sedimentological chronology analysis in lake sediments from Chibuzhang Co, North Tibet (China). *Quat. Geochronol.* **2019**, *52*, 88–102. [CrossRef]

32. Anderson, J.B.; Conway, H.; Bart, P.J.; Witus, A.E.; Greenwood, S.L.; McKay, R.M.; Hall, B.L.; Ackert, R.P.; Licht, K.; Jakobsson, M.; et al. Ross Sea paleo-ice sheet drainage and deglacial history during and since the LGM. *Quat. Sci. Rev.* **2014**, *100*, 31–54. [CrossRef]

33. Xiao, J.; Si, B.; Zhai, D.; Itoh, S.; Lomtatidze, Z. Hydrology of Dali Lake in central-eastern Inner Mongolia and Holocene East Asian monsoon variability. *J. Paleolimnol.* **2008**, *40*, 519–528. [CrossRef]

34. Passega, R. Texture as characteristic of clastic deposition. *AAPG Bull.* **1957**, *41*, 1952–1984.

35. Passega, R. Grain size representation by CM patterns as a geologic tool. *J. Sediment. Res.* **1964**, *34*, 830–847. [CrossRef]

36. Ren, R.; Chen, S.; Dong, P.; Liu, F. Spatial and Temporal Variations in Grain Size of Surface Sediments in the Littoral Area of Yellow River Delta. *J. Coast. Res.* **2012**, *28*, 44–53. [CrossRef]

37. Li, Y.; Yu, H.; Yi, L.; Su, Q.; Hu, K.; Xu, X.; Wang, J. Grain-size characteristics and its sedimentary significance of coastal sediments of the borehole Lz908 in the south Bohai Sea (the Laizhou Bay), China. *Mar. Sci.* **2014**, *38*, 107–113.

38. Zhang, L.; Chen, S.; Pan, S.; Yi, L.; Jiang, C. Sediment variability and transport in the littoral area of the abandoned Yellow River Delta, northern Jiangsu. *J. Geogr. Sci.* **2014**, *24*, 717–730. [CrossRef]

39. Li, Y.; Morrill, C. A Holocene East Asian winter monsoon record at the southern edge of the Gobi Desert and its comparison with a transient simulation. *Clim. Dyn.* **2015**, *45*, 1219–1234. [CrossRef]

40. Han, W.; Lü, S.; Appel, E.; Berger, A.; Madsen, D.; Vandenberghe, J.; Yu, L.; Han, Y.; Yang, Y.; Zhang, T.; et al. Dust Storm Outbreak in Central Asia After ~3.5 kyr BP. *Geophys. Res. Lett.* **2019**, *46*, 7624–7633. [CrossRef]

41. Bond, G.; Kromer, B.; Beer, J.; Muscheler, R.; Evans, M.N.; Showers, W.; Hoffmann, S.; Lotti-Bond, R.; Hajdas, I.; Bonani, G. Persistent Solar Influence on North Atlantic Climate During the Holocene. *Science* **2001**, *294*, 2130–2136. [CrossRef]

42. Jian, Z.; Wang, P.; Saito, Y.; Wang, J.; Pflaumann, U.; Oba, T.; Cheng, X. Holocene variability of the Kuroshio Current in the Okinawa Trough, northwestern Pacific Ocean. *Earth Planet. Sci. Lett.* **2000**, *184*, 305–319. [CrossRef]

43. Cheng, H.; Edwards, R.L.; Sinha, A.; Spötl, C.; Yi, L.; Chen, S.; Kelly, M.; Kathayat, G.; Wang, X.; Li, X.; et al. The Asian monsoon over the past 640,000 years and ice age terminations. *Nature* **2016**, *534*, 640–646. [CrossRef] [PubMed]

44. Bond, G.; Showers, W.; Cheseby, M.; Lotti, R.; Almasi, P.; deMenocal, P.; Priore, P.; Cullen, H.; Hajdas, I.; Bonani, G. A Pervasive Millennial-Scale Cycle in North Atlantic Holocene and Glacial Climates. *Science* **1997**, *278*, 1257–1266. [CrossRef]

45. Yi, L.; Chen, S.; Ortiz, J.D.; Chen, G.; Peng, J.; Liu, F.; Chen, Y.; Deng, C. 1500-year cycle dominated Holocene dynamics of the Yellow River delta, China. *Holocene* **2016**, *26*, 222–234. [CrossRef]

46. Liu, Y.H.; Henderson, G.M.; Hu, C.Y.; Mason, A.J.; Charnley, N.; Johnson, K.R.; Xie, S.C. Links between the East Asian monsoon and North Atlantic climate during the 8,200 year event. *Nat. Geosci.* **2013**, *6*, 117–120. [CrossRef]

47. Liu, D.; Wang, Y.; Cheng, H.; Edwards, R.L.; Kong, X.; Chen, S.; Liu, S. Contrasting Patterns in Abrupt Asian Summer Monsoon Changes in the Last Glacial Period and the Holocene. *Paleoceanogr. Paleoclimatol.* **2018**, *33*, 214–226. [CrossRef]

48. Talley, L.D. Closure of the Global Overturning Circulation Through the Indian, Pacific, and Southern Oceans: Schematics and Transports. *Oceanography* **2013**, *26*, 80–97. [CrossRef]

49. Hsueh, Y.; Schultz, J.R.; Holland, W.R. The Kuroshio flow-through in the East China Sea: A numerical model. *Prog. Oceanogr.* **1997**, *39*, 79–108. [CrossRef]

50. Sun, Y.; Clemens, S.C.; Morrill, C.; Lin, X.; Wang, X.; An, Z. Influence of Atlantic meridional overturning circulation on the East Asian winter monsoon. *Nat. Geosci.* **2012**, *5*, 46–49. [CrossRef]

51. Stevens, T.; Thomas, D.S.G.; Armitage, S.J.; Lunn, H.R.; Lu, H. Reinterpreting climate proxy records from late Quaternary Chinese loess: A detailed OSL investigation. *Earth Sci. Rev.* **2007**, *80*, 111–136. [CrossRef]

52. Xiang, R.; Yang, Z.; Saito, Y.; Guo, Z.; Fan, D.; Li, Y.; Xiao, S.; Shi, X.; Chen, M. East Asia Winter Monsoon changes inferred from environmentally sensitive grain-size component records during the last 2300 years in mud area southwest off Cheju Island, ECS. *Sci. China Ser. D* **2006**, *49*, 604–614. [CrossRef]

53. Steinke, S.; Glatz, C.; Mohtadi, M.; Groeneveld, J.; Li, Q.; Jian, Z. Past dynamics of the East Asian monsoon: No inverse behaviour between the summer and winter monsoon during the Holocene. *Glob. Planet. Chang.* **2011**, *78*, 170–177. [CrossRef]

54. Yancheva, G.; Nowaczyk, N.R.; Mingram, J.; Dulski, P.; Schettler, G.; Negendank, J.F.W.; Liu, J.; Sigman, D.M.; Peterson, L.C.; Haug, G.H. Influence of the intertropical convergence zone on the East Asian monsoon. *Nature* **2007**, *445*, 74–77. [CrossRef] [PubMed]

55. Xiao, J.; Nakamura, T.; Lu, H.; Zhang, G. Holocene climate changes over the desert/loess transition of north-central China. *Earth Planet. Sci. Lett.* **2002**, *197*, 11–18. [CrossRef]

56. Ge, Q.; Xue, Z.; Yao, Z.; Zang, Z.; Chu, F. Anti-phase relationship between the East Asian winter monsoon and summer monsoon during the Holocene? *J. Ocean Univ. China* **2017**, *16*, 175–183. [CrossRef]

57. Hu, B.; Yang, Z.; Zhao, M.; Saito, Y.; Fan, D.; Wang, L. Grain size records reveal variability of the East Asian Winter Monsoon since the Middle Holocene in the Central Yellow Sea mud area, China. *Sci. China Earth Sci.* **2012**, *55*, 1656–1668. [CrossRef]

58. Kang, S.; Du, J.; Wang, N.; Dong, J.; Wang, D.; Wang, X.; Qiang, X.; Song, Y. Early Holocene weakening and mid- to late Holocene strengthening of the East Asian winter monsoon. *Geology* **2020**, *48*, 1043–1047. [CrossRef]